A Cell-Centered Lagrangian Method Based on Local Evolution Galerkin Scheme for Two-Dimensional Compressible Flows

Ming Yu
Key Laboratory for Computational Physics, Institute of Applied Physics and Computational Mathematics
Beijing, China
E-mail: yu_ming@iapcm.ac.cn

Haibo Xu, Yutao Sun
Institute of Applied Physics and Computational Mathematics
Beijing, China
E-mail: xu_haibo@iapcm.ac.cn, syt@iapcm.ac.cn

***Abstract*—This paper presents a new cell-centered Lagrangian method for two-dimensional compressible flows. The main feature of the method is that the velocity and pressure at the cell vertex are computed using the local Galerkin evolution scheme for solving the linearized flow equations in terms of the bicharacteristic theory, and then the velocity and pressure are used to update the grid coordinates and evaluate the numerical flux across the cell interface. The local Galerkin evolution operator gives the solutions evolving for an infinite small time interval from the initial conditions and still can maintain the genuinely multidimensional nature of a hyperbolic system.**

Keywords-Lagrangian method; cell-centered scheme; local evolution Galerkin scheme; finite volume scheme

I. INTRODUCTION

In multimaterial flow simulation, a grid-staggered Lagrangian method is extensively adopted [1]. Recently, increased attention has been paid to the cell-centered Lagrangian method, in which the primary variables including the density, momentum (velocity) and total energy, are defined at the center of a cell. The cell-centered scheme is constructed by integrating directly the system of conservation laws on each moving cell with finite volume discretization, so it can well preserve the conservation of the momentum and total energy, and may not require the artificial viscosity and hourglass viscosity. In addition, it has synchronous time advancement among the flow governing equations. The idea of cell-centered scheme was firstly introduced by Godunov [2] in one-dimensional gas dynamics and then extended to multidimensional flows. The key point of multidimensional cases lies in the determination of the velocity at the cell vertex. There are several typical approaches to determine the vertex velocity of a cell [3]-[6].

Apparently, it is a good idea to construct the Riemann solver of the cell vertex directly from the characteristic property about multidimensional compressible fluid equations. To design this "genuinely multidimensional" numerical solver, the evolution Galerkin scheme [7]-[9] may be adopted, in which the exact integral equations from a general theory of bicharacteristics for the linear or linearized hyperbolic system were derived in terms of the primitive physical variables, and then the vertex solutions were obtained to determine the vertex velocity and evaluate the numerical fluxes across the cell interface. Usually, these integral solutions could be further approximated by approximate evolution operator in such a way that all of the infinitely many directions of propagation of bicharacteristics were explicitly taken into account. This vertex solver from the bicharacteristic theory essentially is a multidimensional Riemann solver or a generalization of the original idea of Godunov to multidimensional hyperbolic conservation laws. The idea has been studied extensively from theoretical as well as numerical point of view and applied to various science and engineering for the compressible fluid equations in the Eulerian formalism [7]-[9]. Traditionally, the evolution Galerkin operator gives the evolutive course within a certain time interval. In order to simplify the computations of the integral solutions and facilitate the semi-discrete finite volume scheme, the local evolution Galerkin operator is proposed by Sun and Ren [9], in which the solutions that are evolved for an infinitely small time interval from the initial condition in terms of the primitive variables are derived by means of a limit operation to let the evolution time approach to zero. The semi-discrete finite volume scheme decouples the temporal discretization and the spatial discretization while maintaining the genuine multidimensional nature of the original evolution Galerkin scheme.

The paper is organized as follows. In Section II, we give the compressible flows equations in the Lagrangian formulation. In Section III, the vertex solver to compute velocity and pressure by local evolution Galerkin operator is derived. In Section IV, the global description of the present algorithm is shown. In Section V, several numerical tests are shown. Some main conclusions are presented in Section VI.

II. NUMERICAL METHOD FOR COMPRESSIBLE LAGRANGIAN FLOW EQUATIONS

A. Governing equations of compressible flow

The governing equations of compressible flow without internal dissipation and external forces can express into the following integrals as the Lagrangian formalism:

$$\frac{d}{dt}\int_{\Omega(t)} \rho d\Omega = 0 \tag{1}$$

$$\frac{d}{dt}\int_{\Omega(t)} \rho \boldsymbol{u} d\Omega = -\int_{\partial\Omega(t)} p d\boldsymbol{l} \tag{2}$$

$$\frac{d}{dt}\int_{\Omega(t)} \rho E d\Omega = -\int_{\partial\Omega(t)} p\boldsymbol{u}\cdot d\boldsymbol{l} \tag{3}$$

$$\frac{d}{dt}\int_{\Omega(t)} d\Omega = -\int_{\partial\Omega(t)} \boldsymbol{u}\cdot d\boldsymbol{l} \tag{4}$$

 ISBN: 978-1-61208-419-0

where ρ is density, u and v are component velocity, p is pressure, E is specific total energy, $E = e + (u^2 + v^2)/2$, e is specific internal energy, and $\Omega(t)$ is a control volume with the boundary $\partial\Omega(t)$, $d\boldsymbol{l}$ is the differential length of the surface for the control volume.

For a given control volume W_c with the mass $m_c = \int_{\Omega_c} \rho d\Omega$ and the area $A_c = \int_{\Omega_c} d\Omega$, a definition about the average value of any physical variable f is $\bar{f}_c = \frac{1}{m_c}\int_{\Omega_c} \rho f d\Omega$. Thus, (1) becomes an algebraic equation $\bar{r}_c A_c = m_c = \text{const}$, and (2)-(4) can be written for these discrete unknowns in two-dimensional space with regard of a vector form:

$$\frac{d\bar{\boldsymbol{U}}_c}{dt} = -\frac{1}{m_c}\int_{\partial\Omega_c} \boldsymbol{H}\cdot\boldsymbol{n} dl \tag{5}$$

where $\bar{\boldsymbol{U}}_c = \left(-\tau_c, u_c, v_c, E_c\right)^T$, $\tau_c = A_c / m_c$, $\boldsymbol{n}$ is the outward unit vector normal to the boundary of the control volume, $\boldsymbol{H} = \left(u, p, 0, pu\right)^T \boldsymbol{i} + \left(v, 0, p, pv\right)^T \boldsymbol{j}$ is the tensor of fluxes.

Under Lagrangian coordinates, the control volume moves with the same velocity as the fluid particle, and the trajectory equations of any fluid particle is:

$$\frac{dx}{dt} = u\,,\ \frac{dy}{dt} = v \tag{6}$$

B. The finite volume scheme

For any nonoverlapping polygons cell with the number $N(c)$ of interfaces of the cell and a interface denoted by I_k, the flow governing equation may be written as:

$$\frac{d\bar{\boldsymbol{U}}_c}{dt} = -\frac{1}{m_c}\sum_{k=1}^{N(c)}\int_{I_k} \boldsymbol{H}_k\cdot\boldsymbol{n}_k dl \tag{7}$$

A suitable approach to solve (7) is the semi-discrete procedure that decouples the temporal discretization and the spatial discretization. Thus, the respective high order scheme about temporal and spatial discretization can be adopted independently. A second-order Runge-Kutta scheme for temporal discretization is following:

$$\begin{aligned}
\bar{\boldsymbol{U}}_c^{*} &= \bar{\boldsymbol{U}}_c^{n} - \frac{\Delta t}{m_c}\sum_{k=1}^{N(c)}\int_{I_k} \boldsymbol{H}_k\left(\boldsymbol{E}_{I,0}\boldsymbol{R}_c\bar{\boldsymbol{U}}_c^{n}\right)\cdot\boldsymbol{n}_k dl \\
\bar{\boldsymbol{U}}_c^{n+1} &= \frac{1}{2}\bar{\boldsymbol{U}}_c^{n} + \frac{1}{2}\left[\bar{\boldsymbol{U}}_c^{*} - \frac{\Delta t}{m_c}\sum_{k=1}^{N(c)}\int_{I_k} \boldsymbol{H}_k\left(\boldsymbol{E}_{I,0}\boldsymbol{R}_c\bar{\boldsymbol{U}}_c^{*}\right)\cdot\boldsymbol{n}_k dl\right]
\end{aligned} \tag{8}$$

where $\boldsymbol{R}_c$ is the reconstruction operator which transforms the cell averages of the conservative variables to their spatial distributions, and $\boldsymbol{E}_{I,0}$ is an approximate Galerkin evolution operator to compute the solution at time $t_n^{+} = t_n + 0$ on cell interface I_k.

The rest part of this section will give the procedures for the reconstruction and the numerical integration of the interface flux in (8), while the approximate Galerkin evolution operator will be discussed in Section III.

C. The reconstructions

Usually, the reconstruction is carried out in terms of the primitive physical variables $\boldsymbol{q} = (\rho, u, v, p)^T$ from the cell average data $\bar{\boldsymbol{q}}_c$. To obtain a spatially first-order scheme, a piecewise constant reconstruction is sufficient; and to obtain a spatially second-order scheme, a piecewise linear reconstruction is sufficient.

D. The numerical integration of the interface flux

In order to give the relation between variables at interface and variables at vertex and ensure the equivalent discretization between the numerical flux across interface and the numerical flux at vertex at the same time, the numerical integration to the interface flux in (8) may adopt the following midpoint rule [6]:

$$\begin{aligned}
&\sum_{k=1}^{N(c)}\int_{I_k} \boldsymbol{H}_k\left(\boldsymbol{E}_{I,0}\boldsymbol{R}_c\bar{\boldsymbol{U}}_c\right)\cdot\boldsymbol{n}_k dl \\
&\quad = \frac{1}{2}\sum_{r=1}^{N(c)}\left[\boldsymbol{H}_r\left(\boldsymbol{E}_0\boldsymbol{R}_c\bar{\boldsymbol{U}}_c\right) + \boldsymbol{H}_{r+1}\left(\boldsymbol{E}_0\boldsymbol{R}_c\bar{\boldsymbol{U}}_c\right)\right]\cdot\boldsymbol{n}_{r,r+1}L_{r,r+1}
\end{aligned} \tag{9}$$

where $\boldsymbol{E}_0$ is the vertex solver from the local Galerkin evolution operator to compute the solution at the cell vertex at time $t_n^{+} = t_n + 0$, and r is the numbering of the vertices counterclockwise, $L_{r,r+1}$ denotes the length of an interface $[M_r, M_{r+1}]$ about the neighbouring vertices M_r and M_{r+1} and $\boldsymbol{n}_{r,r+1}$ denotes the outward unit vector normal to the interface $[M_r, M_{r+1}]$.

III. VERTEX SOLVER $\boldsymbol{E}_0$ BY THE LOCAL EVOLUTION GALERKIN OPERATOR

The central idea of the local evolution Galerkin operator is to compute the theoretical solutions along every bicharacteristic direction for a small time interval from the initial conditions about the hyperbolic equations, and then the theoretical solutions are made some approximate operations and limit operations to obtain the local approximate operator.

In order to derive the theoretical evolution Galerkin solutions about the nonlinear hyperbolic system, a suitable local linearization is usually utilized with regard to the primitive variables, so that the bicharacteristics are reduced to straight lines. For this purpose, we have:

$$\frac{d\boldsymbol{q}}{dt} + \boldsymbol{A}_1(\boldsymbol{q})\frac{\partial\boldsymbol{q}}{\partial x} + \boldsymbol{A}_2(\boldsymbol{q})\frac{\partial\boldsymbol{q}}{\partial y} = 0$$

where $\boldsymbol{q} = \begin{bmatrix}\rho\\ u\\ v\\ p\end{bmatrix}$, $\boldsymbol{A}_1(\boldsymbol{q}) = \begin{bmatrix}0 & \rho & 0 & 0\\ 0 & 0 & 0 & 1/\rho\\ 0 & 0 & 0 & 0\\ 0 & \rho c^2 & 0 & 0\end{bmatrix}$,

$\boldsymbol{A}_2(\boldsymbol{q}) = \begin{bmatrix}0 & 0 & \rho & 0\\ 0 & 0 & 0 & 0\\ 0 & 0 & 0 & 1/\rho\\ 0 & 0 & \rho c^2 & 0\end{bmatrix}$.

The flow equations are linearized by freezing the Jacobian matrices about a reference state $\tilde{\boldsymbol{q}} = (\tilde{\rho}, \tilde{u}, \tilde{v}, \tilde{p})$ at point $\tilde{P} = (\tilde{x}, \tilde{y}, \tilde{t})$. The linearized system with frozen constant Jacobian matrices can be written as:

$$\frac{d\boldsymbol{q}}{dt} + \boldsymbol{A}_1(\tilde{\boldsymbol{q}})\frac{\partial \boldsymbol{q}}{\partial x} + \boldsymbol{A}_2(\tilde{\boldsymbol{q}})\frac{\partial \boldsymbol{q}}{\partial y} = 0 \qquad (10)$$

Considering any unit vector denoted by $\boldsymbol{n}(\theta) = (n_x, n_y)^T = (\cos\theta, \sin\theta)^T$, $\theta \in [0, 2\pi]$, there is a matrix pencil $\boldsymbol{A}(\tilde{\boldsymbol{q}}, \theta) = n_x \boldsymbol{A}_1(\tilde{\boldsymbol{q}}, \theta) + n_y \boldsymbol{A}_2(\tilde{\boldsymbol{q}}, \theta)$, which has four real eigenvalues: $\lambda_1 = \tilde{c}$, $\lambda_{2,3} = 0$, $\lambda_4 = -\tilde{c}$, and four corresponding linearly-independent right eigenvectors $\boldsymbol{r}_1 = \left(-\tilde{\rho}/\tilde{c}, \cos\theta, \sin\theta, -\tilde{\rho}\tilde{c}\right)^T$, $\boldsymbol{r}_2 = \left(1, 0, 0, 0\right)^T$, $\boldsymbol{r}_3 = \left(0, \sin\theta, \cos\theta, 0\right)^T$, $\boldsymbol{r}_4 = \left(\tilde{\rho}/\tilde{c}, \cos\theta, \sin\theta, \tilde{\rho}\tilde{c}\right)^T$. The four right eigenvectors may construct a right eigenmatrix $\boldsymbol{R}$, and the characteristic variables can be define as $\boldsymbol{w} = \boldsymbol{R}^{-1}\boldsymbol{q}$.

Multiplying system (10) by $\boldsymbol{R}^{-1}$ from the left, an eigen-system can be obtained

$$\frac{d\boldsymbol{w}}{dt} + \boldsymbol{R}^{-1}\boldsymbol{A}_1\boldsymbol{R}\frac{\partial \boldsymbol{w}}{\partial x} + \boldsymbol{R}^{-1}\boldsymbol{A}_2\boldsymbol{R}\frac{\partial \boldsymbol{w}}{\partial y} = 0 \qquad (11)$$

Thus, (11) can be transformed into the following quasi-diagonalized system:

$$\frac{d\boldsymbol{w}}{dt} + \boldsymbol{\Lambda}_1\frac{\partial \boldsymbol{w}}{\partial x} + \boldsymbol{\Lambda}_2\frac{\partial \boldsymbol{w}}{\partial y} = \boldsymbol{s} \qquad (12)$$

where

$$\boldsymbol{w} = \begin{bmatrix} w_1 \\ w_2 \\ w_3 \\ w_4 \end{bmatrix} = \begin{bmatrix} \frac{1}{2}(-\frac{p}{\tilde{\rho}\tilde{c}} + u\cos\theta + v\sin\theta) \\ \rho - \frac{p}{\tilde{c}^2} \\ u\sin\theta - v\cos\theta \\ \frac{1}{2}(\frac{p}{\tilde{\rho}\tilde{c}} + u\cos\theta + v\sin\theta) \end{bmatrix},$$

$$\boldsymbol{s} = \begin{bmatrix} s_1 \\ s_2 \\ s_3 \\ s_4 \end{bmatrix} = \begin{bmatrix} \frac{1}{2}\tilde{c}(\sin\theta\frac{\partial w_3}{\partial x} - \cos\theta\frac{\partial w_3}{\partial y}) \\ 0 \\ \tilde{c}\sin\theta(\frac{\partial w_1}{\partial x} - \frac{\partial w_4}{\partial x}) - \tilde{c}\cos\theta(\frac{\partial w_1}{\partial y} - \frac{\partial w_4}{\partial y}) \\ \frac{1}{2}\tilde{c}(-\sin\theta\frac{\partial w_3}{\partial x} + \cos\theta\frac{\partial w_3}{\partial y}) \end{bmatrix},$$

$$\boldsymbol{\Lambda}_1 = diag(\lambda_{1,1}, \lambda_{1,2}, \lambda_{1,3}, \lambda_{1,4}) = \begin{bmatrix} -\tilde{c}\cos\theta & 0 & 0 & 0 \\ 0 & 0 & 0 & 0 \\ 0 & 0 & 0 & 0 \\ 0 & 0 & 0 & \tilde{c}\cos\theta \end{bmatrix},$$

$$\boldsymbol{\Lambda}_2 = diag(\lambda_{2,1}, \lambda_{2,2}, \lambda_{2,3}, \lambda_{2,4}) = \begin{bmatrix} -\tilde{c}\sin\theta & 0 & 0 & 0 \\ 0 & 0 & 0 & 0 \\ 0 & 0 & 0 & 0 \\ 0 & 0 & 0 & \tilde{c}\sin\theta \end{bmatrix}.$$

Equation (12) shows that each characteristic variable w_l (l=1,2,3,4) is evolved along the corresponding bicharacteristic curve:

$$\left(\frac{d\boldsymbol{z}}{dt}\right)_l = \left(\lambda_{1,l}(\theta), \lambda_{2,l}(\theta)\right)^T, l = 1, 2, 3, 4,$$

where $\boldsymbol{z} = (x, y)^T$, according to the relation

$$\frac{Dw_l}{Dt} = \frac{dw_l}{dt} + \lambda_{1,l}(\theta)\frac{\partial w_l}{\partial x} + \lambda_{2,l}(\theta)\frac{\partial w_l}{\partial y} = s_l.$$

Therefore, given the initial condition at time $\tilde{t}$, the solution of w_l at $P = (x, y, \tilde{t} + \tau)$ is:

$$w_l(x, y, \tilde{t} + \tau, \theta) = w_l[x - \lambda_{1,l}(\theta)\tau, y - \lambda_{2,l}(\theta)\tau, \tilde{t}] + \hat{s}_l(\theta) \qquad (13)$$

where

$$\hat{s}_l(\theta) = \int_{\tilde{t}}^{\tilde{t}+\tau} s_l[x - \lambda_{1,l}(\theta)(\tilde{t} + \tau - \xi), y - \lambda_{2,l}(\theta)(\tilde{t} + \tau - \xi), \xi]d\xi.$$

For any given angle θ, the four bicharacteristic curves from $P(x, y, \tilde{t} + \tau)$ denoted by $C_l(\theta)$ are depicted in Figure 1. The $C_1(\theta)$ or $C_4(\theta)$, for θ from 0 to 2π, generates a bicharacteristic cone or Mach cone, and the $C_2(\theta)$ or $C_3(\theta)$ is perpendicular to the bottom of the cone. The intersection point between $C_l(\theta)$ and the initial plane with $\tilde{P}(\tilde{x}, \tilde{y}, \tilde{t})$ is denoted by $Q_l(\theta)$. For $\theta \in [0, 2\pi]$, the $Q_1(\theta)$ and $Q_4(\theta)$ locate in the circle with the center point $\tilde{P}(\tilde{x}, \tilde{y}, \tilde{t})$ and the radius $\tilde{c}\tau$, and $Q_4(\theta) = Q_1(\theta + \pi)$, moreover, the $Q_2(\theta)$ and $Q_3(\theta)$ locate in the initial point $\tilde{P}(\tilde{x}, \tilde{y}, \tilde{t})$, and $Q_2(\theta) = Q_3(\theta)$. So, the expressions may hold: $Q_{1,4}(\theta) = (x \pm \tilde{c}\tau\cos\theta, y \pm \tilde{c}\tau\sin\theta, \tilde{t})$, $Q_{2,3}(\theta) = (x, y, \tilde{t})$.

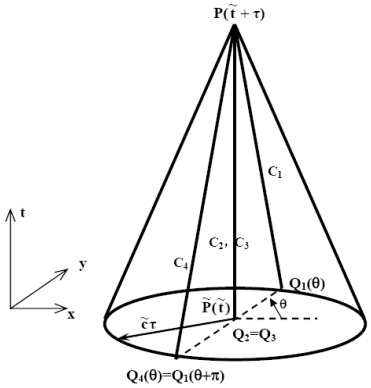

Figure 1. Bicharacteristic curves and bicharacteristic cone

Equation (13) can be also written in vector form as

$$\boldsymbol{w}(P, \theta) = \begin{pmatrix} w_1(Q_1(\theta)) \\ w_2(Q_2(\theta)) \\ w_3(Q_3(\theta)) \\ w_4(Q_4(\theta)) \end{pmatrix} + \begin{pmatrix} \hat{s}_1(\theta) \\ \hat{s}_2(\theta) \\ \hat{s}_3(\theta) \\ \hat{s}_4(\theta) \end{pmatrix}. \qquad (14)$$

Multiplying (14) with the right eigenmatrix $\boldsymbol{R}$ from the left and then integrating with respect to θ from 0 to 2π, it leads to:

$$\boldsymbol{q}(P)=\frac{1}{2\pi}\int_0^{2\pi}\left[\sum_{l=1}^{4}\boldsymbol{r}_l\left(w_l\left(Q_l(\theta)\right)+\hat{s}_l(\theta)\right)\right]d\theta\,.$$

The symmetries in characteristic variables and the source terms are used to obtain the solutions of the linearized hyperbolic system:

$$\begin{aligned}u(P)&=\frac{1}{2}u(\tilde{P})\\&+\frac{1}{2\pi}\int_0^{2\pi}\left[-\frac{p(Q_1)}{\tilde{\rho}\tilde{c}}\cos\theta+u(Q_1)\cos^2\theta+v(Q_1)\sin\theta\cos\theta\right]d\theta\\&+\frac{1}{2\pi}\int_0^{2\pi}\int_{\tilde{t}}^{\tilde{t}+\tau}S[\boldsymbol{z}+\tilde{c}(\tilde{t}+\tau-\xi)\boldsymbol{n}(\theta),\xi,\theta]\cos\theta d\xi d\theta\\&-\frac{1}{2\tilde{\rho}}\int_{\tilde{t}}^{\tilde{t}+\tau}\frac{\partial p(\boldsymbol{z},\xi)}{\partial x}d\xi\end{aligned}\tag{15}$$

$$\begin{aligned}v(P)&=\frac{1}{2}v(\tilde{P})\\&+\frac{1}{2\pi}\int_0^{2\pi}\left[-\frac{p(Q_1)}{\tilde{\rho}\tilde{c}}\sin\theta+u(Q_1)\cos\theta\sin\theta+v(Q_1)\sin^2\theta\right]d\theta\\&+\frac{1}{2\pi}\int_0^{2\pi}\int_{\tilde{t}}^{\tilde{t}+\tau}S[\boldsymbol{z}+\tilde{c}(\tilde{t}+\tau-\xi)\boldsymbol{n}(\theta),\xi,\theta]\sin\theta d\xi d\theta\\&-\frac{1}{2\tilde{\rho}}\int_{\tilde{t}}^{\tilde{t}+\tau}\frac{\partial p(\boldsymbol{z},\xi)}{\partial y}d\xi\end{aligned}\tag{16}$$

$$\begin{aligned}p(P)&=\frac{1}{2\pi}\int_0^{2\pi}\left[p(Q_1)-\tilde{\rho}\tilde{c}u(Q_1)\cos\theta-\tilde{\rho}\tilde{c}v(Q_1)\sin\theta\right]d\theta\\&-\frac{1}{2\pi}\tilde{\rho}\tilde{c}\int_0^{2\pi}\int_{\tilde{t}}^{\tilde{t}+\tau}S[\boldsymbol{z}+\tilde{c}(\tilde{t}+\tau-\xi)\boldsymbol{n}(\theta),\xi,\theta]d\xi d\theta\end{aligned}\tag{17}$$

where $S(\boldsymbol{z},t,\theta)=\tilde{c}\left[\frac{\partial u(\boldsymbol{z},t,\theta)}{\partial x}\sin^2\theta+\frac{\partial v(\boldsymbol{z},t,\theta)}{\partial y}\cos^2\theta\right]$

$-\frac{\tilde{c}}{2}\left[\frac{\partial u(\boldsymbol{z},t,\theta)}{\partial y}+\frac{\partial v(\boldsymbol{z},t,\theta)}{\partial x}\right]\sin 2\theta$.

For discretized grids, we assume that there are M control volumes with a common vertex $\boldsymbol{z}=(x,y)^T$, and θ_{ka} and θ_{kb} respectively are the starting and ending angles of the kth $k(k\le M)$ grid about the common vertex, thus (15)-(17) can be rewritten into:

$$\begin{aligned}u(P)&=\frac{1}{2}u(\tilde{P})\\&+\frac{1}{2\pi}\sum_{k=1}^{M}\int_{\theta_{ka}}^{\theta_{kb}}\left[-\frac{p(Q_1)}{\tilde{\rho}\tilde{c}}\cos\theta+u(Q_1)\cos^2\theta+v(Q_1)\sin\theta\cos\theta\right]d\theta\\&+\frac{1}{2\pi}\sum_{k=1}^{M}\int_{\theta_{ka}}^{\theta_{kb}}\int_{\tilde{t}}^{\tilde{t}+\tau}S[\boldsymbol{z}+\tilde{c}(\tilde{t}+\tau-\xi)\boldsymbol{n}(\theta),\xi,\theta]\cos\theta d\xi d\theta\\&+\frac{1}{2\tilde{\rho}}\int_{\tilde{t}}^{\tilde{t}+\tau}\frac{\partial p(\boldsymbol{z},\xi)}{\partial x}d\xi\end{aligned}\tag{18}$$

$$\begin{aligned}v(P)&=\frac{1}{2}v(\tilde{P})\\&+\frac{1}{2\pi}\sum_{k=1}^{M}\int_{\theta_{ka}}^{\theta_{kb}}\left[-\frac{p(Q_1)}{\tilde{\rho}\tilde{c}}\sin\theta+u(Q_1)\cos\theta\sin\theta+v(Q_1)\sin^2\theta\right]d\theta\\&+\frac{1}{2\pi}\sum_{k=1}^{M}\int_{\theta_{ka}}^{\theta_{kb}}\int_{\tilde{t}}^{\tilde{t}+\tau}S[\boldsymbol{z}+\tilde{c}(\tilde{t}+\tau-\xi)\boldsymbol{n}(\theta),\xi,\theta]\sin\theta d\xi d\theta\\&-\frac{1}{2\tilde{\rho}}\int_{\tilde{t}}^{\tilde{t}+\tau}\frac{\partial p(\boldsymbol{z},\xi)}{\partial y}d\xi\end{aligned}\tag{19}$$

$$\begin{aligned}p(P)&=\frac{1}{2\pi}\sum_{k=1}^{M}\int_{\theta_{ka}}^{\theta_{kb}}\left[p(Q_1)-\tilde{\rho}\tilde{c}u(Q_1)\cos\theta-\tilde{\rho}\tilde{c}v(Q_1)\sin\theta\right]d\theta\\&-\frac{1}{2\pi}\tilde{\rho}\tilde{c}\sum_{k=1}^{M}\int_{\theta_{ka}}^{\theta_{kb}}\int_{\tilde{t}}^{\tilde{t}+\tau}S[\boldsymbol{z}+\tilde{c}(\tilde{t}+\tau-\xi)\boldsymbol{n}(\theta),\xi,\theta]d\xi d\theta\end{aligned}\tag{20}$$

Equations (18)-(20) are the exact evolution Galerkin solutions for the linearized Lagrangian flow equations. For simplifying the computation of the integrals including pressure gradient term and source term, some approximate operations are required with the similar procedure [9]. And then, the local Galerkin evolution operator $\boldsymbol{E}_0$ about (18)-(20) at time $t_n^+=t_n+0$ is obtained to make the limit operations with $\tau\to 0$. From Figure 1, the effect of $\tau\to 0$ is to make $P\to\tilde{P}$ and $Q\to\tilde{P}$ and the length of the arc with two end points $Q(\theta_{ib})$ and $Q(\theta_{ie})$ tends to zero. Thus, we have $\boldsymbol{q}\left(Q(\theta)\right)\to\boldsymbol{q}_i$, for $\theta_{ib}\le\theta\le\theta_{ie}$, where $\boldsymbol{q}_i$ is the vector of the primitive variables at $\tilde{P}$ evaluated in terms of the reconstruction in the control volume containing the arc with two end points $Q(\theta_{ib})$ and $Q(\theta_{ie})$.

After approximate and limit operations, the analytical expressions of the vertex solver $\boldsymbol{E}_0$ by the local Galerkin evolution operator are the following:

$$\begin{aligned}u(P)&=\frac{1}{\pi}\sum_{i=1}^{N}\left[-\frac{p_i}{\tilde{\rho}\tilde{c}}(\sin\theta_{ie}-\sin\theta_{ib})\right.\\&\left.+u_i\left(\frac{\theta_{ie}-\theta_{ib}}{2}+\frac{\sin 2\theta_{ie}-\sin 2\theta_{ib}}{4}\right)-v_i\frac{\cos 2\theta_{ie}-\cos 2\theta_{ib}}{4}\right]\end{aligned}\tag{21}$$

$$\begin{aligned}v(P)&=\frac{1}{\pi}\sum_{i=1}^{N}\left[\frac{p_i}{\tilde{\rho}\tilde{c}}(\cos\theta_{ie}-\cos\theta_{ib})\right.\\&\left.-u_i\frac{\cos 2\theta_{ie}-\cos 2\theta_{ib}}{4}+v_i\left(\frac{\theta_{ie}-\theta_{ib}}{2}-\frac{\sin 2\theta_{ie}-\sin 2\theta_{ib}}{4}\right)\right]\end{aligned}\tag{22}$$

$$\begin{aligned}p(P)&=\frac{1}{2\pi}\sum_{i=1}^{N}\left[p_i(\theta_{ie}-\theta_{ib})\right.\\&\left.-\tilde{\rho}\tilde{c}u_i(\sin\theta_{ie}-\sin\theta_{ib})+\tilde{\rho}\tilde{c}v_i(\cos\theta_{ie}-\cos\theta_{ib})\right]\end{aligned}\tag{23}$$

It was found that the vertex solver $\boldsymbol{E}_0$ is able to take multidimensional effect into account in a natural way, and to consider the effect of the different sonic impedences to straightway apply to multimaterial flows, and to be fully competent for the structured or unstructured grids.

 ISBN: 978-1-61208-419-0

IV. DESCRIPTION OF THE PRESENT ALGORITHM

Step 1: Initialization

At time $t = t^n$, the geometrical coordinates x_i^n , y_i^n ($i = 1,2,\cdots,I$) of each vertex of each cell and the physical variables $\overline{\rho}_k^n$ ($\overline{\tau}_k^n$), $\overline{u}_k^n$, $\overline{v}_k^n$, $\overline{E}_k^n$, $\overline{p}_k^n$ ($k = 1,2,\cdots,K$) at center of each cell are known.

Step 2: Reconstruction

The physical primitive variables at each vertex of each cell are obtained by means of the formula in Subsection II.C.

Step 3: Vertex solver

The velocities u_i^n , v_i^n and pressure p_i^n ($i = 1,2,\cdots,I$) at each vertex of each cell are obtained by means of (21)-(23) for the local Galerkin evolution operator $\boldsymbol{E}_0$.

Step 4: Update of the geometrical quantities

The updated grids and the length and outward vector of each interface are achieved from the new coordinate data x_i^{n+1} , y_i^{n+1} ($i = 1,2,\cdots,I$) of each vertex of each cell.

Step 5: Update of the physical variables

The physical variables $\overline{\tau}_k^{n+1}$, $\overline{u}_k^{n+1}$, $\overline{v}_k^{n+1}$, $\overline{E}_k^{n+1}$ at center of the updated grids can be computed from (8), and then the corresponding $\overline{p}_k^{n+1}$ is obtained from the equation of state.

V. NUMERICAL RESULTS

A. Multimaterial Sod's shock tube problem

The initial conditions of two kinds of perfect gases with different adiabatic indexes are: $(\rho, u, p, \gamma) = (1, 0, 1, 7/5)$ in the left-hand side and $(\rho, u, p, \gamma) = (0.125, 0, 0.1, 5/3)$ in the right-hand side. The density solution at time $t = 0.2$ is shown in Figure 2 for the second-order scheme with CFL=0.8 under different meshes. It can be found that the smaller the grid used, the closer the numerical solution approaches to the exact solution, and there is not unphysical oscillation nearby the shock wave, the rarefaction fan is correctly described. An undershoot appears at the density discontinuity about the contact discontinuity, it is an indigenous property to Lagrangian method.

B. Sedov problem

A highly intense shock wave generated by a strong explosion propagates outward. The perfect gas with adiabatic index $\gamma = 5/3$ is initially at rest for $(\rho, u, p) = (1, 0, 0)$ but an energy spike is set as 182.09 at the center, and all the boundary conditions are solid walls. The 30×30 uniform Cartesian meshes in computational domain $[0,1.1] \times [0,1.1]$ are used with CFL=0.8. Figure 3(a-b) shows the calculated meshes and density contours by the second-order scheme at time *t*=1, and Figure 4(a-b) shows the density profile by the first-order and the second-order scheme at time *t*=1. It is found that the second-order scheme has an improved precision on the first-order scheme, and the second-order scheme still has excellent resolution and symmetry.

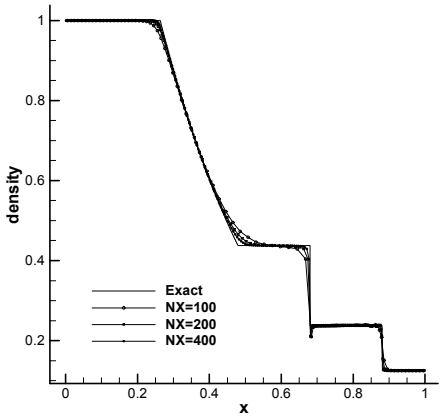

Figure 2. Comparison of numerical solution for Sod's shock tube with exact solution for second-order scheme

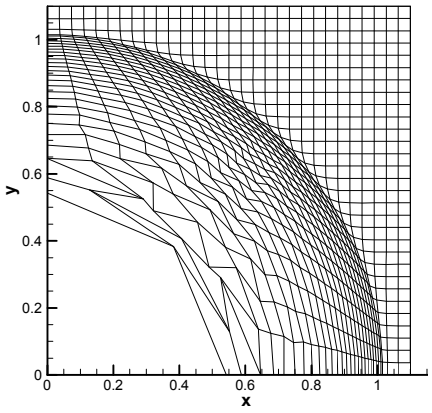

(a) Meshes variation

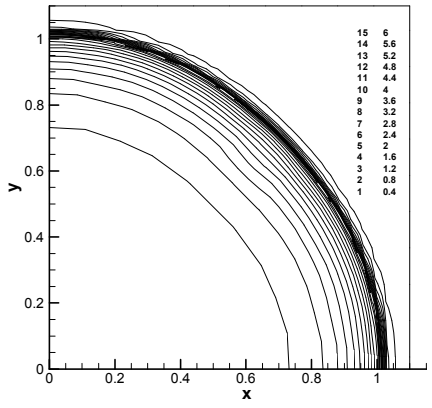

(b) Density contours

Figure 3. Solution of 2nd order scheme for Sedov problem at time *t*=1

C. Saltzman problem

A planar shock wave located initially at $x = 0$ moves rightward on the perfect gas with $\gamma = 5/3$, and the front state of shock wave is $(\rho, u, p) = (1, 0, 0)$. When the piston velocity at the left-hand is set as $u = 1$, the exact propagation velocity of shock wave should be $4/3$. A computational domain $[0,1.0] \times [0,0.1]$ on Cartesian coordinates with grid

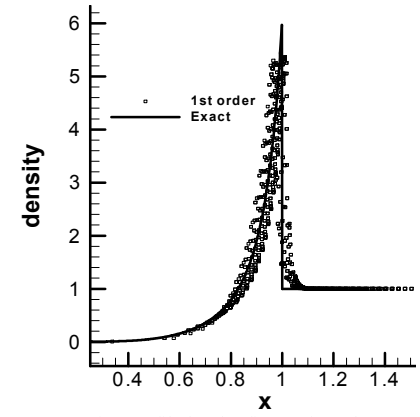

(a) Density profile by the first order scheme

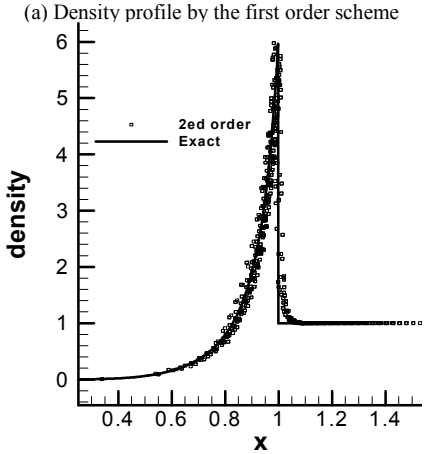

(b) Density profile by the second order scheme

Figure 4. Density solution for Sedov problem at time t=1

number 100×10 is taken, and a uniform meshes in y direction and a nonuniform meshes with the mapping $x = i\Delta x + (0.1 - j\Delta y)\sin(i\Delta x\pi)$ in x direction are used, meanwhile, the boundary condition at the left-hand is an invariable velocity and all the other boundaries are set as solid wall. Obviously, the shock wave will reflect on the right-hand wall at time t=0.75. The meshes and density contours at time t=0.84 are shown in Figure 5 about the reflected shock wave. It can be found that the one-dimensional property of the reflected shock wave can be well preserved. The robustness of this scheme is also powerfully demonstrated by the test case.

VI. CONCLUSION AND FUTURE WORK

A cell-centered Lagrangian method for 2D compressible flows is present on basis of the local evolution Galerkin scheme under semi-discrete finite volume framework where the vertex velocity is computed in a coherent manner with the numerical fluxes across the cell interface. The main feature of this method is the physical variables at vertex of a cell are computed by virtue of the bicharacteristics theory about the linearized flow equations, which is essentially a multidimensional Riemann solver taking "multidimensional effect" into account in a natural way. Our future most important works will be on the extension to arbitrary Lagrangian-Eulerian method.

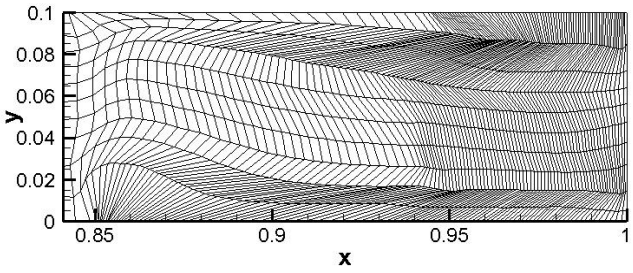

(a) Meshes

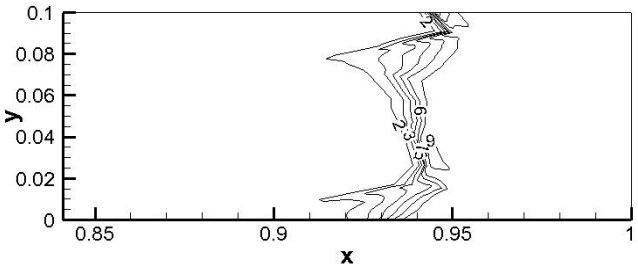

(b) Density contours

Figure 5. Computational results about Salzman problem at t=0.84

ACKNOWLEDGMENT

This work was supported under Grant-11272064 of Natural Science Foundation of China.

REFERENCES

[1] M. Wilkins, "Calculation of Elastic-Plastic Flow, in Methods in Computational Physics", vol.3, Academic Press, New York, 1964, pp. 211-263.

[2] R. Ritchtmyer and K. Morton, Difference Methods for Initial-Value Problems, John Wiley, New York, 1967.

[3] J. Dukowicz and B. Meltz, "Vorticity Errors in Multidimensional Lagrangian Codes", Journal of Computational Physics, 99, 1992, pp. 115–134.

[4] C. Juan and S. Chi-Wang, "A High Order ENO Conservative Lagrangian Type Scheme for the Compressible Euler Equations", Journal of Computational Physics, 227, 2007, pp. 1567-1596.

[5] B. Després and C. Mazeran, "Lagrangian Gas Dynamics in Two Dimensions and Lagrangian Systems", Arch. Rational Mech. Anal., 178, 2005, pp. 327–372.

[6] P. Maire, R. Abgrall and J. Breil, "A Cell-Centered Lagrangian Scheme for Two-Dimensioanl Compressible Flow Problems", SIAM Journal of Scientific Computing, 29(4), 2007, pp. 1781-1824.

[7] M. Lukáčová-Medvid'ová, K. Morton and G. Warnecke, "Evolution Galerkin Methods for Hyperbolic Systems in Two Space Dimensions", Mathematics of Computation, 69(232), 2000, pp. 1355-1384.

[8] M. Lukáčová-Medvid'ová, J. Saibertová and G. Warnecke, "Finite Volume Evolution Galerkin Methods for Nonlinear Hyperbolic Systems", Journal of Computational Physics, 183, 2002, pp. 533–562.

[9] Y. Sun and Y.-X. Ren, "The Finite Volume Local Evolution Galerkin Method for Solving the Hyperbolic Conservation Laws", Journal of Computational Physics, 228, 2009, pp. 4945-4960.

 ISBN: 978-1-61208-419-0